RSC Advances

PAPER

View Article Online
View Journal | View Issue

Cite this: *RSC Adv.*, 2017, **7**, 47592

Novel layer-by-layer self-assembled peptide nanocarriers for siRNA delivery†

Betül Bozdoğan, [a] Öznur Akbal, ‡[ab] Ekin Çelik, ‡[cd] Mustafa Türk [e] and Emir Baki Denkbaş *[f]

All complex and functional structures of nature consist of simple building blocks that are thermodynamically balanced and self-assembled at the molecular level. Production of functional bio-nanomaterials with molecular self-assembly mechanisms, based on a bottom-up approach, has become increasingly important in recent years. In this study, a biodegradable and biocompatible siRNA nanocarrier system, consisting of diphenylalaninamide (FFA) based nanoparticles, was developed for silencing of HER2, a gene known to be overexpressed in breast cancer. FFA contains an amide functional group that has a dipolar nature with zero net charge. Here we report an original approach to functionalizing peptide nanoparticles based on layer-by-layer polyelectrolyte deposition (LbL PD) technique. The resulting well-defined FFA nanoparticles (FFANPs) were coated with polycationic poly-L-lysine (PLL) by cation–dipole interaction, giving rise to a net positive surface charge. The PLL coating improved the physical stability of FFANPs at physiological pH and temperature. The cationized FFANP was then interacted with the polyanionic siRNA, forming an FFANP–PLL/siRNA complex. Nanoparticles were then interacted with PLL one more time, to create a third layer that can prevent degradation of the siRNA by nucleases and achieve effective delivery of the siRNA into the cytoplasm. These original FFANP–PLL/siRNA/PLL were optimized to achieve efficient *in vitro* gene silencing. Overall, this study shows that FFANP–PLL/siRNA/PLL are promising gene carriers for gene silencing therapies.

Received 31st July 2017
Accepted 3rd October 2017

DOI: 10.1039/c7ra08460a

rsc.li/rsc-advances

Introduction

RNA interference (RNAi) is a commonly studied gene silencing mechanism that uses siRNAs to prevent protein expression at the post-transcriptional level. Although there are many materials used as nanocarriers, challenges in the effective delivery of siRNAs are not yet fully overcome.[1] siRNA delivery systems such as liposomes and polymeric nanoparticles are mainly used, some of which are made from self-assembled materials.[2–4] Self-assembly is the most basic mechanism involved in the formation of many structures in nature. It is also a fabrication method for nanocarriers, especially for those with biomolecules (proteins, peptides, lipids, and DNAs) as building blocks. Therefore, by using environmental triggers (such as pH, temperature, and light), biomolecules have often been used to design "smart carriers" for delivering bioactive agents, particularly in living systems.[5–9] Self-assembly of peptides was first shown with surfactant-like peptides containing a hydrophilic head and hydrophobic tail, forming peptide nanosphere structures.[10]

Amyloid-derived peptides are the most important peptides used for self-assembly into nanostructures. Amyloid peptides are mainly associated with amyloidosis diseases like Alzheimer's, Prion, Parkinson's, Creutzfeldt–Jakob's, and type-II diabetes. Deposition of β-amyloid peptide (Aβ) on tissues and organs leads to the development of neurodegenerative disorders.[11] Diphenylalanine (FF) peptide, the structural motif of the β-amyloid polypeptide, is currently being used as a building block for nanocarrier fabrication. Many studies with FF dipeptides and their derivatives (such as cationic FF, Fmoc-FF, and Boc-FF) report that this peptide can be organized into rings, ellipses, discs, and bowls outside of spherical or tubular structures.[12,13] The self-assembly process depends on the concentration and the precise balance of interactions between peptide–peptide and peptide–water molecules. The FF nanostructures are stable due to T-shaped aromatic stacking, intermolecular hydrogen bonds between peptide–peptide, and peptide–water hydrogen bonds. Their simple structure, ease of chemical modification,

[a]*Nanotechnology and Nanomedicine Division, Hacettepe University, Beytepe, Ankara, Turkey*
[b]*Polatlı Faculty of Art and Sciences, Gazi University, Polatli, Ankara, Turkey*
[c]*Bioengineering Division, Hacettepe University, Beytepe, Ankara, Turkey*
[d]*Advanced Technologies Application and Research Center, Hacettepe University, Beytepe, Ankara, Turkey*
[e]*Department of Bioengineering, Faculty of Engineering, Kirikkale University, Kirikkale, Turkey*
[f]*Chemistry Department, Hacettepe University, Beytepe, Ankara, Turkey. E-mail: denkbas@hacettepe.edu.tr*

† Electronic supplementary information (ESI) available. See DOI: 10.1039/c7ra08460a

‡ These authors contributed equally.

biocompatibility, and ability to be regulated under different conditions have led to a great deal of interest in FF peptides as drug delivery systems.[14–16] Yan *et al.* were the first to show that cationic FF molecules can be used as gene and drug carriers by regulating the nanovesicles at physiological pH.[17,18] Cationic FF molecules have been the subject of many studies to investigate their applications as carriers or sensor components. They can be arranged into nanoparticles with molecular self-assembly mechanisms under different stimuli and conditions.[19,20] However, a common problem encountered in all these studies is that the resulting peptide nanoparticles are not stable, and they can change their morphology to accommodate changing ambient conditions. Zhang *et al.* were the first to develop stable FF-based nanostructures for use as drug carriers.[21] These stable nanostructures exhibit high biocompatibility and superior biodegradability.

In this report, nanoparticles were prepared with diphenylalaninamide (FFA), a derivative of FF dipeptide. These nanoparticles were investigated for the successful delivery of siRNA to the HER2 gene in a human breast cancer cell line. To overcome the challenges of siRNA delivery, FFA nanoparticles (FFANPs) were modified using the layer-by-layer polyelectrolyte deposition (LbL PD) technique. The LbL PD technique relies on the adsorption mechanism in a multi-layered approach, in which at least two types of polymers having affinity for each other are attached to the surface.[22,23] In this study, polycationic poly-L-lysine (PLL) was added for FFANP dispersion and it adsorbed to the nanoparticle surface by cation–dipole interaction to create the first layer. Then, FFANPs cationized with the PLL layer were interacted with polyanionic siRNA to form the second layer. To form the third layer, nanoparticles were again coated with PLL, which provided a positive charge to the FFANPs. The third layer also protected the siRNA molecule from nuclease activity and facilitated its cellular uptake. Entrapment efficiency (EE) and loading capacity (LC) of siRNA in the nanoparticles was evaluated also release studies were performed. The ability of the designed nanoparticles to be used as a siRNA carrier was assessed by measuring HER2 gene expression levels of BT-474 cells transfected with these nanoparticles. Furthermore, immunocytochemistry studies were carried out to support the results obtained. To the best of our knowledge, this is the first report of the synthesis of stable self-assembled FF-based nanoparticles modified with PLL for use in gene delivery.

Experimental

Chemicals

FFA (H-Phe-Phe-$NH_2 \cdot HCl$) was purchased from Bachem (Bubendorf, Switzerland). HFIP (1,1,1,3,3,3-hexafluoro-2-propanol) was purchased from Merck (Darmstadt, Germany); glutaraldehyde (GA) and α-poly-L-lysine hydrobromide (α-PLL, M (monomer, Lys·HBr, $C_6H_{13}N_2OBr$) = 209.09 g mol^{-1}, M_w = 15 000–30 000 g mol^{-1}) were purchased from Sigma-Aldrich (St. Louis, MO, USA). Instead of the molar concentration of PLL, the molar concentration of the lysine repeating units was used in measurements. Stock PLL solution (22 mM) was dialyzed against dH_2O to remove toxic hydrobromide. All reagents were commercially available and used without further purification unless otherwise noted. Ultrapure water with a resistivity of 18.2 MΩ was used in all experiments.

Synthesis and characterization of FFANPs

Synthesis. FFANPs were prepared as described previously by Zhang *et al.* with minimal modification.[21] In the typical procedure, 1 mg of FFA dipeptide was dissolved in 8 μL HFIP to prepare a stock FFA solution (freshly prepared in every experiment). Then, 1 mL of 0.06% GA solution was added to achieve crosslinking (FFA : GA = 1 : 1). The solution was then incubated at room temperature overnight to complete cross-linking and self-assembly. The solution became cloudy with formation of the nanoparticles. Finally, the resulting suspension was ultracentrifuged (12 000 rpm, 10 min) and washed with ultrapure water three times to remove excess HFIP and residual GA. The FFANPs were kept in ultrapure water at 4 °C for use in further experiments.

Morphological characterization of FFANPs. FFANP morphology was confirmed by scanning and transmission electron microscopy (SEM and TEM, respectively). SEM images were obtained with an EVO 50 EP microscope (Carl Zeiss, Oberkochen, Germany) operated with an electron beam energy of 10 keV. In brief, the samples were prepared by casting 5 μL of FFANP suspension on silicon wafers and dried under nitrogen gas, and then coated with gold. TEM was performed using a JEM 1220 microscope (JEOL, Peabody, MA, USA) operated with an electron beam energy of 100 keV. To prepare the samples, 5 μL of FFANP suspension was placed onto a copper grid and dried in vacuum. The average particle size distributions were calculated in SEM and TEM images using ImageJ (NIH Image).

FTIR analyses of FFANPs. Attenuated total reflection-Fourier transform infrared (ATR-FTIR) analysis was performed with a Nicolet™ iS™ 50 spectrometer (Thermo Fisher Scientific, Madison, WI, USA). Scans were between 4000 and 600 cm^{-1} at a resolution of 4 cm^{-1}.

Mass spectroscopy analyses of FFANPs. Mass spectra of FFANPs were recorded with a Voyager-DE Pro MALDI-TOF (matrix-assisted laser desorption/ionization-time of flight) instrument (Applied Biosystems, Foster City, CA, USA). Desorption and ionization of the samples were carried out at a pressure of about 10^{-7} Torr using a 337 nm output from a pulsed nitrogen laser (Spectra Physics, Santa Clara, CA, USA). Twenty-five kV acceleration potential was applied for ion extraction. All measurements were recorded and calibrated with an average of 500 laser pulses in positive and linear mode. Alpha-cyano-4-hydroxycinnamic acid (CHCA) and 2,5-dihydroxybenzoic acid (DHB) matrices were arranged in acetonitrile : water (1 : 1, v/v) at a concentration of 10 mg mL^{-1}. MALDI samples were prepared by mixing peptides to be analysed with aforementioned matrices (1 : 5, v/v). Subsequently, 0.5 μL of this mixture was dropped on the sample plate and dried at room temperature.

Dynamic light scattering (DLS) analyses of FFANPs. DLS analyses of the nanoparticles were carried out on a Zetasizer Nano ZS instrument (Malvern Instruments, Malvern, UK). The results were recorded in ultrapure water at 25 °C and 173° backscatter angle (with viscosity: 0.8872 cP, refractive index:

1.33, dielectric constant: 78.5). The electrophoretic mobility of the 1 mg mL^{-1} nanoparticle solution was measured and this value was converted to zeta potential and size values by the Helmholtz–Smoluchowski equation.

Preparation and characterization of FFANPs as gene carrier by layer-by-layer polyelectrolyte deposition

LbL assembly was employed to coat FFA nanoparticles to achieve siRNA transport. In brief, to prepare the first polycation layer on the nanoparticle surface, a stock PLL solution (22 mM) was added drop by drop to the FFANP dispersion (1 mg mL^{-1}) at different ratio of amide groups of FFA to amine groups of PLL (Ad/An) under constant stirring. The mixture was incubated under constant stirring in a dark at room temperature for 2 h to complete adsorption. After incubation, the nanoparticles were precipitated (12 000 rpm, 10 min) and washed 3 times to remove unbound and weakly bound PLL. This prevented undesired complexes between free PLL and siRNA during the adsorption of the next polyelectrolyte layer. Later, to coat with the second layer, stock polyanion siRNA solution (6.7 μM) was added dropwise to the FFANP-PLL dispersion. Final concentrations of siRNA were 27, 50, 100, 130, 200, and 260 nM. After the mixture was incubated for 2 h under constant stirring at room temperature, the resulting FFANP–PLL–siRNA was precipitated (12 000 rpm, 10 min), washed 3 times, and resuspended in ultrapure water. To determine entrapment efficiency (EE) and loading capacity (LC) of siRNA in the nanoparticles, supernatants from washing step were collected and measured for siRNA content using a Ribogreen kit (Thermo Fisher Scientific, Waltham, MA, USA) according to the manufacturer's protocol. EE and LC were calculated as previously reported.[24]

The final PLL coating was applied to the FFANP–PLL–siRNA as mentioned previously. LbL PD was evaluated by zeta potential measurements, SEM analyses, and statistical calculations using the ImageJ program on images obtained from SEM analyses.

Release studies of siRNA from gene carriers

Release of siRNA from the FFANP–PLL/siRNA and FFANP–PLL/siRNA/PLL was evaluated in buffer solutions with pH 7.4 (0.01 M phosphate buffer, PB), pH 5.5 (0.01 M acetate buffer), and pH 4.0 (0.01 M acetate buffer). RNAse-free water was used to prepare the buffer solutions. The pHs were chosen to mimic the blood pH (7.4), endosomal pH (6.0–5.5), and lysosomal pH (4.5–4.0). Briefly, siRNA loaded nanoparticles were suspended in buffer solution (1 mg mL^{-1}) and incubated in a 37 °C shaking water bath for 48 hours. At each predetermined time point, the nanoparticle suspensions were centrifuged (12 000 rpm, 10 min). The 100 μL of the supernatants from each nanoparticle suspension were collected and their siRNA contents were stained with fluorescence using Ribogreen kit. The fluorescence intensity was measured by CLARIOstar microplate reader (BMG Labtech, Germany). According to the standard curve of siRNA, the percentage of cumulatively released siRNA was calculated.

Statistical analysis

Experiments were performed in triplicate unless otherwise indicated. Data were analysed using descriptive statistics and presented as mean values ± standard deviation from independent measurements unless otherwise indicated. Statistical comparisons between different treatments were assessed by one-way ANOVA, assuming significance at $p < 0.05$.

In vitro degradation of FFANP and FFANP–PLL

To determine pH-dependent degradation behaviour of FFANP and FFANP–PLL, the following buffer systems were used: pH 7.4 (0.01 M phosphate buffer, PB), pH 5.5 (0.01 M acetate buffer), and pH 4.0 (0.01 M acetate buffer). Briefly, FFANPs were dispersed in the buffer solutions (2 mg per 10 mL) and incubated at 37 °C in the dark for 4 weeks. The turbidity change of nanoparticle dispersions at different time intervals was analysed by a TB 300 IR turbidimeter (Lovibond, Dortmund, Germany). In addition, to check the effect of temperature on the degradation of nanoparticles, FFANP dispersions in ultrapure water were incubated at 4 °C, 25 °C, and 37 °C and turbidity measurements were taken at different time intervals.

Enzymatic degradation of FFANP and FFANP–PLL were carried out with trypsin-EDTA (0.25%, Sigma-Aldrich). To do this, nanoparticles at 2 mg mL^{-1} in PBS pH 7.4 were incubated with 50 μL of trypsin-EDTA and a trace amount of NaN_3 (to protect the trypsin from microorganisms) at 37 °C for a week. The degradation results were evaluated with SEM analysis.

Cell culture

The HER2-overexpressed human breast cancer cell line, BT-474 (HTB-20, ATCC), was used in cell culture experiments. Cells were cultured in 25 cm^2 flasks with Dulbecco's modified Eagle's medium (DMEM, Sigma-Aldrich), including 10% fetal bovine serum (FBS, Sigma-Aldrich) and 1% L-glutamine (Sigma-Aldrich) and incubated at 37 °C in 5% CO^2 humidified atmosphere.

Cytotoxicity

Cytotoxic effects of nanoparticles were evaluated with an XTT (2,3-bis-(2-methoxy-4-nitro-5-sulfophenyl)-2*H*-tetrazolium-5-carboxanilide) assay. Briefly, BT-474 cells were seeded in 96-well plates (5×10^3 cells per mL) and cultured. After 24 h, the medium was aspirated and fresh medium with a different concentration and formulation of nanoparticles was added to the wells and incubated for 24 h. The medium in every well was replaced with 25 μL of XTT reagent (1 mg mL^{-1} in PBS) and incubated at 37 °C for 4 h. Cell viability was determined by measuring the absorbance at 450 nm.

In vitro siRNA transfection

Transfection studies were performed with two different methods. For transfection with HER2 siRNA (FlexiTube, Qiagen, Hilden, Germany) cells (5×10^4 cells per well) were seeded with antibiotic-free medium in six-well plates 12 h prior to transfection. In the first method, cells were bombarded with 200 μL

of 5-fold concentrated gene carrier in serum- and antibiotic-free medium (Transfection Medium, TM) to prevent unwanted protein adsorption to the nanoparticle surface. After 4 h, the wells were diluted 5-fold with serum-containing medium so that final carrier concentration was 1, 2, and 3 mg mL^{-1}. In the second method, transfection agents were prepared directly with the serum-containing medium so that final carrier concentration was 1, 2, and 3 mg mL^{-1}. After 24 h incubation, the medium was replaced with fresh medium. Forty-eight hours after transfection, cells were harvested for cytotoxicity and PCR analysis. Seventy-two hours after transfection cells were collected for immunocytochemistry assay.

Polymerase chain reaction (PCR) experiments

RNA isolation and cDNA synthesis were performed with the RNeasy Mini Kit (Qiagen) and QuantiTect Rev. Transcription kits (Qiagen) according to the manufacturer's protocol. Quantitative gene expression analysis was performed with the Viia 7 real-time PCR system (Applied Biosystems) with Qiagen's QuantiTect primer assays and SYBR green master mix. Results were analysed using the $\Delta\Delta C_T$ method, *via* the system's software.

Immunocytochemistry

HER2 protein expression was assessed with primary antibody staining (Affymetrix, Santa Clara, CA, USA) *via* an HRP kit (HRP (RTU), Thermo Scientific), prior to AEC staining (GBI Labs, Bothell, WA, USA). Backgrounds were stained with hematoxylin after antibody staining. Slides were visualized under a light microscope.

Results and discussion

Synthesis and characterization of FFANPs

In this study, FFA was crosslinked with GA molecules to form peptide nanoparticles. The amide carbonyl group of diphenylalanine has strong electron attractive forces because of the double bond between carbon and the electronegative oxygen atom and the attraction of the nonbonded electrons (NBEs) of nearby nitrogen, inducing a conjugate system where these electrons act as delocalized electrons. In this case, it is more convenient to address the molecule as two or more resonance forms, instead of one (Fig. 1A). Delocalization phenomena indicate electron density is diffused in a broad area, where these electrons are in constant movement, ensuring the molecule has high resonance stability. The electron attractive force of this conjugated system hinders the interaction of nitrogen atoms with electrophiles. In addition, the electron delocalization that is formed limits the electrophilic nature of the carbonyl groups at amides, causing the amide group to have the weakest reactivity among the functional groups.[25]

GA is an aggressive carbonyl compound and is known as an amine reactive homobifunctional crosslinker. Its aldehyde groups at both end form bonds with amine groups of proteins *via* Schiff base (–C═N–) formation. Oligomeric GA molecules formed by the aldol reaction form Schiff base bonds with the reactive amine

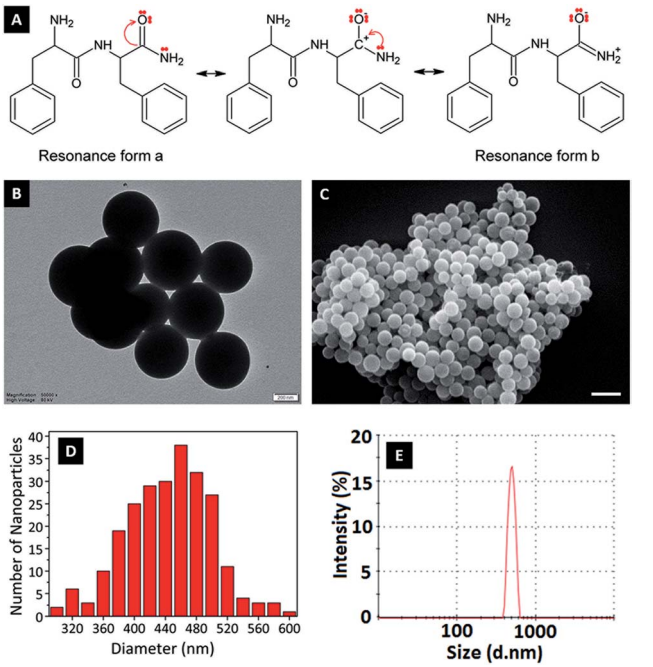

Fig. 1 (A) Resonance delocalization of NBEs of nitrogen in FFA dipeptides and resonance form a and b of FFA. (B) TEM image (scale bar: 200 nm) and (C) SEM image (scale bar: 1 μm) of FFANPs. (D) A histogram of size distribution based on SEM measurement ($n = 260$) and (E) size distribution of FFANP measured by DLS.

ends of FFA molecules, resulting in FFA–$(GA)_2$–FFA and FFA–$(GA)_3$–FFA dimers. Therefore, the resultant FFA dimers have amide functional groups at both ends. As mentioned in the literature crosslinked dimers self-assemble to form peptide nanoparticles *via* nucleation-controlled growth.[21,26]

Morphological characterization of FFANPs. Nanoparticle morphology was evaluated by SEM and TEM analysis. The homogenous contrast that was created by the nanoparticles around their periphery is the typical signature of solid nanoparticles in TEM analysis (Fig. 1B). The average size of the FFANPs was 447.6 ± 51.3 nm and they are shown to be spherical monosized particles according to SEM analysis (Fig. 1C and D). TEM images support the findings of SEM analysis, revealing a spherical structure of the nanoparticles with an average diameter of 460 nm. Synthesized FFANPs were analysed with DLS and their average hydrodynamic radii are shown to be 470 nm, with a polydispersity index of 0.088 (Fig. 1E).

FTIR characterization of FFANPs. FTIR analysis was performed to determine intramolecular interactions and amide bands of nanoparticles. There are 9 primary IR bands related to the structure of proteins. These are amide A, amide B, and amide I–VII bands.[27,28] Fig. 2A shows amide A, B, I, and II bands in IR spectra of FFA dipeptides, FFA–$(GA)_n$–FFA dimers, and FFANP. Two peaks at 3432 and 3359 cm^{-1} representing NH_2 stretching of primary amines, the shoulder at 3307 cm^{-1}, which is an overtone of the absorption at 1603 cm^{-1}, and the strong absorption of NH bending at 1571 cm^{-1} disappeared after crosslinking with GA. GA crosslinking also caused a decrease in the $–NH_2$ bending intensity

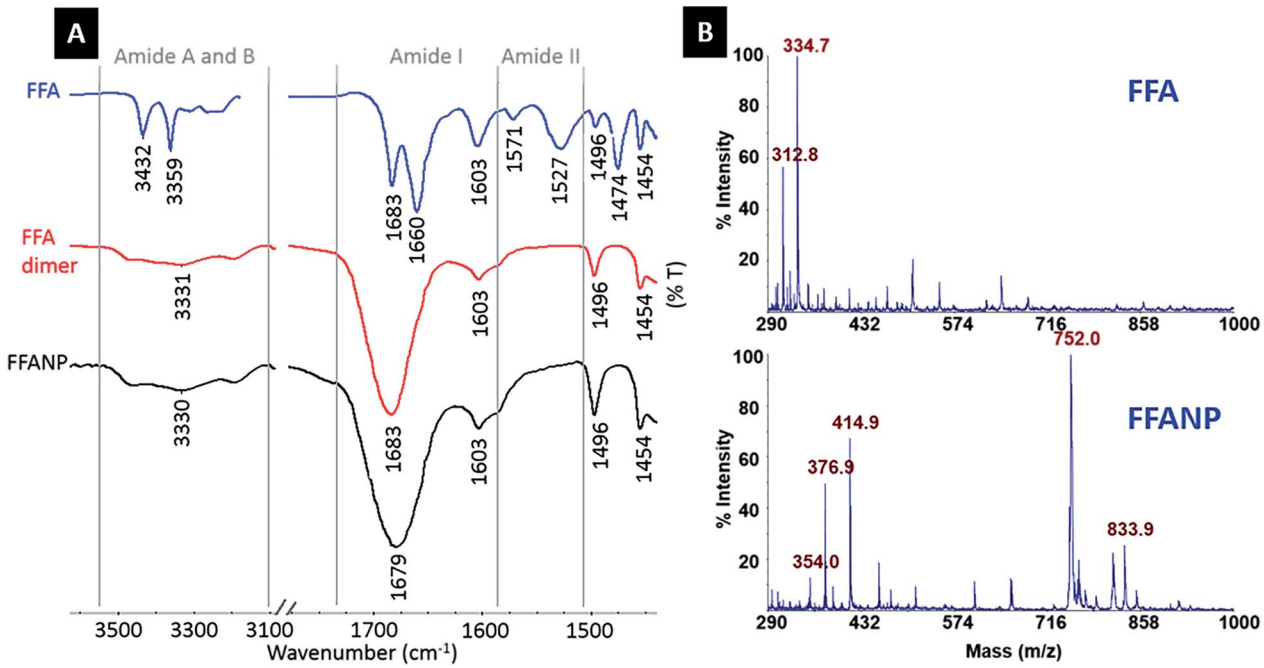

Fig. 2 (A) FTIR spectra of FFA dipeptide, FFA dimers, and FFANPs. (B) MALDI-MS spectra of FFA dipeptide, FFA dimers.

at 1603 cm^{-1}. These findings prove that crosslinking between GA and the FFA dipeptide was successful.

Amide I (C═O stretching) and amide II (N–H bending) bands are commonly used to interpret changes in protein structure and conformation. As mentioned previously, the C═O stretching vibrations of FFA structures seen at 1683 cm^{-1} and 1660 cm^{-1} form the amide I band, together with $-NH_2$ bending vibration at 1603 cm^{-1}. Vibrations representing –NH bending at 1571 cm^{-1} and 1527 cm^{-1} form the typical amide II band.

Absorption at 1660 cm^{-1} on the amide I band and 1527 cm^{-1} and 1571 cm^{-1} on the amide II band of the FFA dipeptide (blue spectrum) indicate β-turn secondary structures, whereas the absorption peak at 1683 cm^{-1} on the amide I band is correlated with antiparallel β-sheet formation.[29–32] The absorption at 1660 cm^{-1} is higher than the absorption at 1683 cm^{-1}, indicating the dominance of the β-turn configuration in the FFA dipeptide. After crosslinking with GA, absorption disappears at 1527, 1571, and 1660 cm^{-1} and increases at the 1683 cm^{-1} peak in FFA–$(GA)_n$–FFA (red spectrum) and FFANP (black spectrum) spectra, proving adaptation of an antiparallel β-sheet arrangement.[21,32–34] This shows that the FFA dipeptide has a structural transition through crosslinking with GA, during nanoparticle formation.

The H-bond is one of the possible forces that may be effective in the self-assembly of the FF dipeptide to a nanostructure.[35–37] There is a strong correlation between C═O stretching frequency and its H-bonding capacity and C═O stretching frequency is a sensitive infrared vibrational spectral marker.[38] H-bond formation is correlated with a 3–30 cm^{-1} red shifting and a broadening and increasing of frequency intensity.[28,38–40] The amide I regions of FFA–$(GA)_n$–FFA and FFANPs are shown in Fig. 2A. Red shift on C═O absorbance at 1683 cm^{-1} to 1679 cm^{-1}, together with broadening of frequency and increase in intensity indicates hydrogen bonding of C═O. Amide A and B bands, demonstrating NH stretching frequency levels, are also important for the interpretation of the H-bonding ability of peptides. It is well established that the non-hydrogen bonded N–H is due to higher energy bands, while the lower energy bands correspond to intramolecularly hydrogen bonded N–H.[37,41] Large absorption peaks seen at amide A and B regions of FFA dimers and FFANP and low-frequency shoulders indicates the presence of hydrogen bonding of the N–H group.[35,42]

Urea ($CO(NH_2)_2$), as a strong H-bonding donor, is commonly used as a hydrogen bonding inhibitor and protein denaturing agent.[43,44] FFANPs were incubated with urea to determine the driving force for the self-assembly mechanism. FFANPs were denatured after incubation in urea, implicating hydrogen bonds in the formation of nanoparticles (Fig. S1†).

Mass spectroscopy analysis of FFANPs. MALDI-MS mass spectra are given in Fig. 2B. The peaks at 313 and 334 *m*/*z* belong to FFA and $FFANa^+$ molecules, respectively. However, both of the peaks seem to diminish at the mass spectrum of FFANPs and two new peaks occur at 752 *m*/*z* and 833 *m*/*z*, representing FFA–$(GA)_2$–FFA and FFA–$(GA)_3$–FFA, respectively. This result indicates the oligomerization of the GA molecule *via* an aldol reaction and dimerization of FFA molecules *via* crosslinking of oligomeric GA.[21]

Zeta potential measurements of FFANPs. Surface charge is an important characteristic for bio-nanomaterials. A methodology used to measure the electrical surface charge is to measure zeta potential.[45] The zeta potential of FFANPs against water at pH 7 is measured as -13.6 ± 6.4 mV ($n = 157$) (Fig. 3A). Although it is known that these particles have zero net charge,

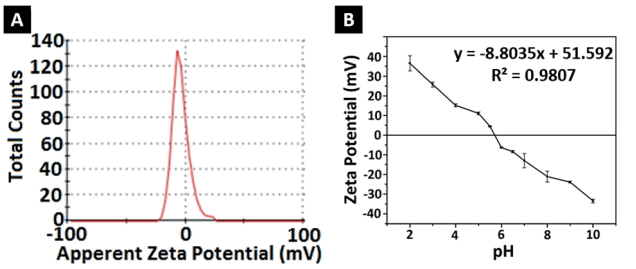

Fig. 3 (A) Zeta potential of FFANPs and (B) zeta potential change *versus* pH.

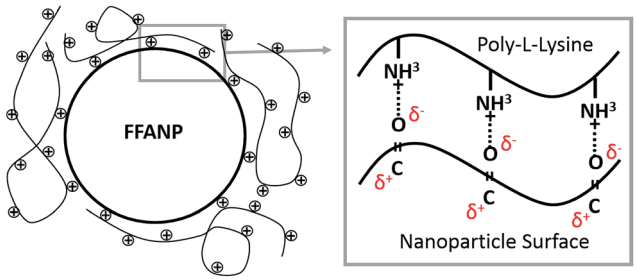

Fig. 4 Schematic representation of the cation–dipole interaction between FFANP and PLL molecules.

the anionic character is thought to be caused by the dipolar nature of the amide groups.

To determine the effect of pH change on the surface charges, zeta potentials of nanoparticles were measured in solutions with different pH (Fig. 3B). At low pH, nanoparticles gained a positive charge due to protonation of oxygen atoms at amide groups. Basic medium caused deprotonation of NH_2 in amide groups, causing a negative surface charge.

Synthesis and characterization of FFANP as a gene carrier

The attempts for adsorption of siRNA molecules directly onto surface of the FFANPs failed due to the lack of positively charged groups on the surface of the nanoparticles (data not shown). FFANPs were further enhanced with polycationic PLL molecules by the LbL PD technique in order to load siRNA.[43,46,47] FFANPs were improved with PLL to cationize.[48] The highly electronegative oxygen atoms in the FFANPs have a lone pair of electrons. Therefore, these oxygen atoms have a strong tendency to combine or associate with H^+ through cation–dipole interactions.[49–51] The main driving force in the assembly of the PLL layer on the FFANP surface is probably the cation–dipole interaction between the positively charged PLL chain and the electronegative amide oxygen atoms of FFANPs (Fig. 4). Gene carriers were then created by electrostatic interactions between FFANP–PLL and siRNA molecules.

Charge deposition on the surface of nanoparticles in LbL PD applications can be verified with zeta potential measurements.[52] In the LbL PD technique, polyelectrolyte adsorption continues until surface neutralization and nanoparticle charge is reversed when there is sufficient polyelectrolyte nearby.[53] FFANPs–PLL formed at different Ad/An ratios were tested to determine their zeta-potentials (Fig. 5A). Nanoparticle surface charge was neutralized quickly at 18/1 ratio, and the surface charge increased linearly with increasing concentrations of PLL. This indicates that PLL is accumulating on the nanoparticle surface. Thickness of the adsorbed layer depends on the selected substrate and chemical structure of the polymer, but it mainly relies on the polymer saturation of the surface.[23] At a Ad/An ratio of 1/1, the surface became saturated; as excess PLL concentrations did not change the zeta potentials. We conclude that PLL molecules cannot be attached to the surface of the nanoparticles due to electrostatic and steric hindrances.

It is known that the LbL PD technique increases nanoparticle diameter until polymer saturation occurs.[54] Fig. 5B shows the

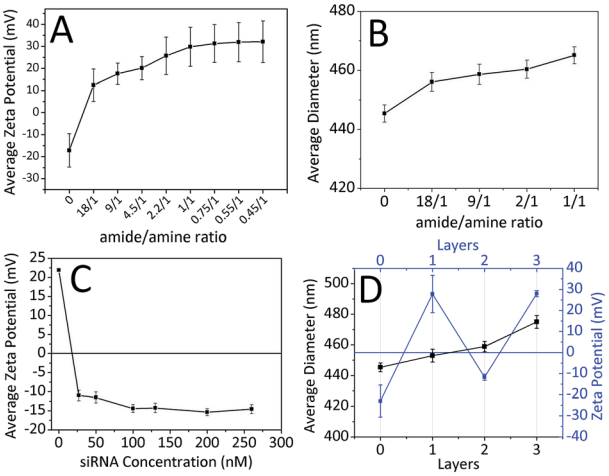

Fig. 5 The effect of PLL concentration on the average zeta potential (A) and average diameter (B) of nanoparticles. The effect of siRNA concentration on the average zeta potential (C) of nanoparticles. The change of average diameter (black curve) and zeta potential (blue curve) after every deposition process and the characteristic zigzag shape of zeta potential during LbL PD (D). Error bars in graph B represent standard error of mean (SEM).

mean diameters of nanoparticles calculated from SEM images using ImageJ software. The first increase in mean diameter (11 nm) occurred at 18/1 ratio. Mean nanoparticle diameter continued to increase with increasing PLL concentration up to a 20 nm when the surface was saturated.

FFANPs were interacted with the polyanionic siRNA layer following coating with the polycationic PLL layer. Fig. 5C shows the difference in zeta potentials of the nanoparticles with increasing siRNA concentration. We conclude that siRNA molecules caused a charge reversal at the surface of the nanoparticles due to interaction with the amine groups of PLL. Zeta potential appeared to increase until surface saturation occurred at 100 nM siRNA concentration.

Quantification of siRNA loading in nanoparticles was evaluated by fluorescence staining. The effects of different siRNA concentrations on loading kinetics were given in Table 1. The results are compatible with results of zeta potential and particle size analysis. According to the table, at the concentrations of 27 nM and 50 nM, the siRNA rapidly binds to the surface of the nanoparticle with 89.25% and 48.57% entrapment efficiency, respectively. As the surface of the nanoparticle reached

Table 1 Effect of different siRNA concentrations on entrapment efficiency (EE) and loading capacity (LC) of FFANP–PLL

Added siRNA (nM)	Added siRNA ($\mu g\ mL^{-1}$)	Loaded siRNA[a] ($\mu g\ mL^{-1}$)	% EE	% LC
27	0.08	0.07 ± 0.00	89.2	0.007
50	0.15	0.07 ± 0.00	48.6	0.007
100	0.31	0.07 ± 0.02	23.8	0.007
130	0.41	0.13 ± 0.03	30.9	0.012
200	0.62	0.16 ± 0.02	25.2	0.015
260	0.83	0.21 ± 0.02	25.8	0.021

[a] Data are presented as mean ± S.D ($n = 3$).

saturation, the adsorption of siRNA slowed down and efficiency decreased. When these results are taken in consideration, nanoparticles interacted with 50 nM siRNA, which are showing the most optimum surface properties, size and loading kinetics, were used in subsequent experiments.

To protect siRNA from nuclease activity and to facilitate their cellular uptake, FFANP–PLL/siRNAs were coated with an additional layer of PLL. The zeta potential values during LbL PD showed the characteristic zigzag shape (Fig. 5D). This demonstrates that oppositely charged molecules successfully accumulate on the nanoparticle surface.

Release studies of siRNA from gene carriers

The amount of released siRNA at different pHs were determined as well. The percentages of total siRNA released over time from nanoparticles were presented in Fig. 6. Accordingly, the siRNA amount released from degraded layers of FFANP–PLL/siRNA (Fig. 6A) and FFANP–PLL/siRNA/PLL (Fig. 6B) increased with the decreased pH. While 70, 52, and 48% of siRNA was released from FFANP–PLL/siRNA within the 4 hours at pH 4, 5.5, and 7.4, respectively; 76, 58, and 49% of siRNA was released from FFANP–PLL/siRNA/PLL. At 20th hour, siRNA release continued from both nanoparticles at pH 7.4 and 5.5, while siRNA was released completely at pH 4. There is no considerable difference between the siRNA release profiles of two nanoparticle formulations. These release profiles of siRNA showed that the release of siRNA from both nanoparticles was slow, sustained, and pH-dependent, which was contributed to prolonging the efficacy of siRNA and rapidly releasing of siRNA by pH-change at target position.

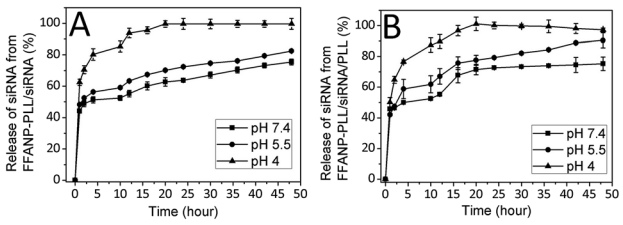

Fig. 6 % Release of siRNA from (A) FFANP–PLL/siRNA and (B) FFANP–PLL/siRNA/PLL at different pH.

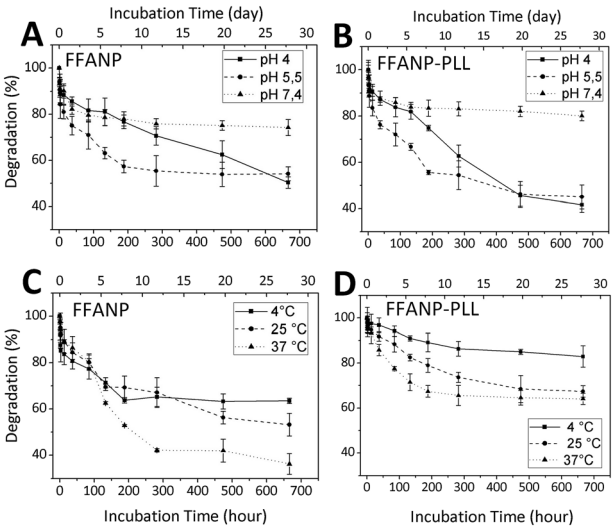

Fig. 7 The effect of pH (A and B) and temperature (C and D) on degradation of FFANP and FFANP–PLL.

In vitro degradation of FFANP and FFANP–PLL

Degradation studies of nanoparticles were performed between pH 4 and 7.4 and between temperatures of 4 and 37 °C. The results are given in Fig. 7. Degradation rates were elevated at decreasing pH for both FFANP (Fig. 7A) and FFANP–PLL (Fig. 7B). PLL modification increased the stability of FFANPs at physiological pH, but their degradation increased dramatically with decreasing pH. This is because, at low pH, the NH_2 groups in the PLL side chains become ionized and the resulting electrostatic repulsion forces cause conformational changes in the PLL molecules.[55] These results demonstrate the nanoparticles' ability of endosomal escape from cellular vesicles, which have a pH of 5–6.[56,57] In addition, the degradation rate of both FFANP (Fig. 7C) and FFANP–PLL (Fig. 7D) increased with increasing temperature. The modification with PLL remarkably improved FFANP stability with temperature change.

To evaluate the enzymatic effect of peptidase on the FFANP and FFANP–PLL were incubated with trypsin. Trypsin degraded the nanoparticles as expected seen on SEM images (Fig. S2†).

Toxicity analysis of gene carriers

Biocompatibility of both FFANP and FFANP–PLL were assessed with XTT experiments on the BT-474 cell line. None of the nanoparticles showed cytotoxicity (Fig. S3†). Toxicity of siRNA-loaded gene carriers was also tested on BT-474 cells. Results showed that the gene carriers are biocompatible and non-toxic for human cells (Fig. 8A–C).

Gene expression analysis

Different gene carrier formulations were tested for their ability to silence the HER2 gene in the breast cancer cell line, BT-474. The studies were planned in several steps to cover all parameters affecting gene expression. Initially, different gene silencing transfection methods were investigated. In the first method,

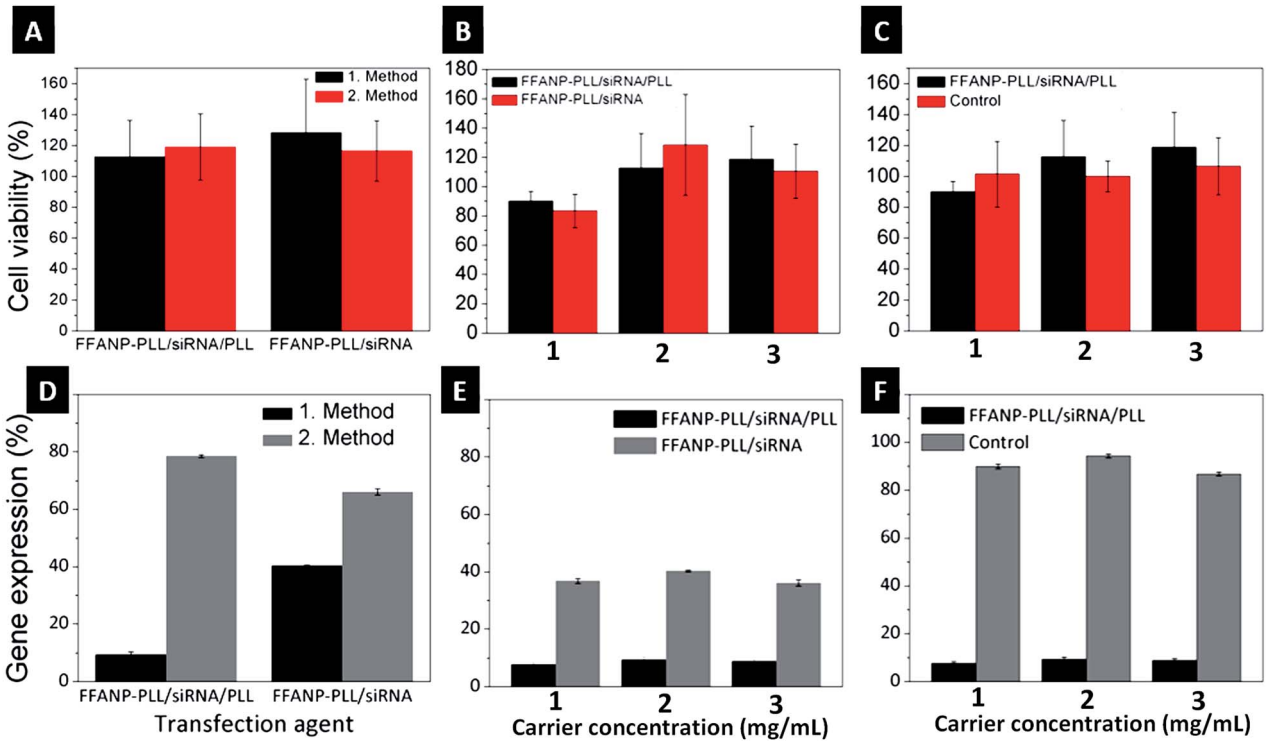

Fig. 8 (A) The effect of two different transfection methods (A), two different gene carrier formulations (B), and three different concentrations of siRNA-loaded gene carrier (C) on BT-474 cell viability. Comparison of two different transfection methods (D), two different gene carrier formulations (E), and three different concentrations of gene carrier (F) on gene silencing.

a concentrated transfection medium (TM) was prepared by dispersing the two gene carrier formulations (FFANP–PLL/siRNA and FFANP–PLL/siRNA/PLL) in serum-free medium. In the second method, gene carriers were dispersed in serum-containing medium. Cells were then bombarded with these concentrated TMs. As seen in Fig. 8D, the first method was more effective than the second method. The result is thought to be caused by both the bombardment of cells with a higher concentration of gene carriers and less aggregation of the gene carriers in serum-free medium.

In further experiments, two different gene carrier formulations were evaluated for their gene silencing ability (Fig. 8E). FFANP–PLL/siRNA/PLL gene carriers had more impact on gene silencing compared with FFANP–PLL/siRNA in all concentrations, concurring with previous work showing that a higher positive charge leads to better gene silencing.[57–59] This is mainly owing to the easier cellular uptake of gene carriers through the negatively charged cellular membrane. In addition, a positive charge facilitates their release into the cytoplasm *via* endosomal escape, allowing them to function. The second layer of PLL on the siRNAs may also protect it from enzymatic activity.

Different concentration of gene carrier contain 50 : 1 (nM siRNA : mg particles) siRNA were tested to define the optimal effective carrier concentration (Fig. 8F). For this purpose, 1, 2, and 3 mg mL^{-1} of gene carriers were interacted with cells so that the final siRNA concentration was 50, 100, and 150 nM, respectively. mRNA expression decreased significantly in the cells incubated with 1 mg mL^{-1} gene carriers, whereas 2 and

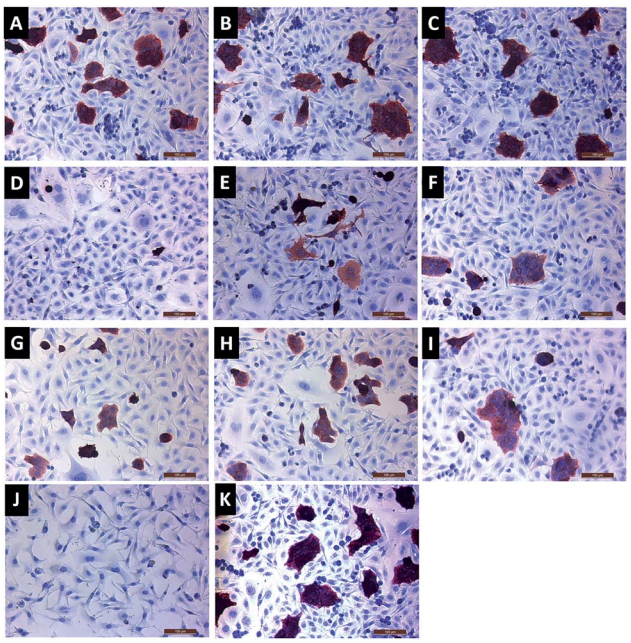

Fig. 9 Light microscopy images of immunocytochemical staining of BT-474 cells with HER2 antibody. Cells transfected with 1 (A), 2 (B), and 3 (C) mg mL^{-1} FFANP–PLL/siRNA gene carriers; with 1 (D), 2 (E), and 3 (F) mg mL^{-1} FFANP–PLL/siRNA/PLL gene carriers. 50 (G), 100 (H), and 150 (I) nM naked siRNA as control groups. (J) Cells without staining as negative control and (K) cells without transfection.

3 mg mL^{-1} did not appear to be as effective. Each concentration was tested with naked siRNA controls at the same concentration. It is well known that an excess amount of siRNA causes off-target effects, leading to silencing of random genes other than HER2.[60] These results show that the FFANP–PLL/siRNA/PLL is effective even at concentrations as low as 1 mg mL^{-1} to be used as gene carrier in gene silencing experiments.

Immunocytochemistry of transfection agents

Immunocytochemistry staining was performed with a HER2 antibody to visualize relative protein expression after 72 h incubation with HER2-specific siRNA-loaded gene carriers (Fig. 9). Red staining in cells represents HER2 protein expression. As seen in Fig. 9D, 1 mg mL^{-1} FFANP–PLL/siRNA/PLL gene carriers, which contain 50 nM siRNA, showed the lowest HER2 expression level. These results are consistent with our gene expression data.

Conclusions

In conclusion, we have successfully established a novel monodispersed, self-assembled, biocompatible, and biodegradable diphenylalanine-based nanoparticle for use as a gene carrier. It is a well-known fact that the main problem of self-assembled nanostructures is their instability. Here, we used GA cross-linked FFA nanocarriers for siRNA-mediated gene silencing. This work is novel because, to the best of our knowledge, it is the first study using the highly efficient and recently preferred LbL PD technique to functionalize FFANPs. In this technique, nanoparticles were cationized with PLL coating. By this modification, the amino groups of PLL are found to be crucial to accomplish siRNA loading. It is thought that by increasing the number of PLL and siRNA layers, the potential of nanocarriers for the delivery of large quantities of silencing agents can be improved. The potent *in vitro* efficacy of these gene carriers indicates that these nanoparticles have the potential to be a robust and useful treatment tool *in vivo*.

Future work will concentrate on using these self-assembled and LbL-modified systems for developing hybrid agents for co-delivery of different siRNAs for cancer therapy. These nanocarriers may possess an efficient synergetic anticancer effect by employing RNA interference-mediated silencing in addition to the anticancer drug-mediated treatment.

Conflicts of interest

The authors declare no conflict of interest.

Acknowledgements

The authors gratefully acknowledged the supports from Rotalab Scientific Instruments Ltd. Co.

References

1 H. Ma, J. Fei, Y. Cui, J. Zhao, A. Wang and J. Li, *Chem. Commun.*, 2013, **49**, 9956–9958.
2 K. Kim, Y. S. Lee and R. W. Carthew, *RNA*, 2007, **13**, 22–29.
3 Y. Dorsett and T. Tuschl, *Nat. Rev. Drug Discovery*, 2004, **3**, 318–329.
4 M. E. Davis, J. E. Zuckerman, C. H. Choi, D. Seligson, A. Tolcher, C. A. Alabi, Y. Yen, J. D. Heidel and A. Ribas, *Nature*, 2010, **464**, 1067–1070.
5 T. Tanaka, A. Legat, E. Adam, J. Steuve, J. S. Gatot, M. Vandenbranden, L. Ulianov, C. Lonez, J. M. Ruysschaert, E. Muraille, M. Tuynder, M. Goldman and A. Jacquet, *Eur. J. Immunol.*, 2008, **38**, 1351–1357.
6 M. Ouali, J. M. Ruysschaert, C. Lonez and M. Vandenbranden, *Mol. Membr. Biol.*, 2007, **24**, 225–232.
7 R. Koynova, Y. S. Tarahovsky, L. Wang and R. C. MacDonald, *Biochim. Biophys. Acta, Biomembr.*, 2007, **1768**, 375–386.
8 V. V. Kumar, C. Pichon, M. Refregiers, B. Guerin, P. Midoux and A. Chaudhuri, *Gene Ther.*, 2003, **10**, 1206–1215.
9 E. Çelik, C. Bayram, R. Akçapınar, M. Türk and E. B. Denkbaş, *J. Bioact. Compat. Polym.*, 2016, **31**, 498–512.
10 S. Vauthey, S. Santoso, H. Gong, N. Watson and S. Zhang, *Proc. Natl. Acad. Sci. U. S. A.*, 2002, **99**, 5355–5360.
11 B. B. Pala, T. Vural, F. Kuralay, T. Çırak, G. Bolat, S. Abacı and E. B. Denkbaş, *Appl. Surf. Sci.*, 2014, **303**, 37–45.
12 C. Guo, Y. Luo, R. Zhou and G. Wei, *ACS Nano*, 2012, **6**, 3907–3918.
13 S. Maity, S. Nir and M. Reches, *J. Mater. Chem. B*, 2014, **2**, 2583–2591.
14 X. Yan, P. Zhu, J. Fei and J. Li, *Adv. Mater.*, 2010, **22**, 1283–1287.
15 R. Huang, S. Wu, A. Li and Z. Li, *J. Mater. Chem. A*, 2014, **2**, 1672–1676.
16 Q. Li, H. Ma, Y. Jia, J. Li and B. Zhu, *Chem. Commun.*, 2015, **51**, 7219–7221.
17 X. Yan, Q. He, K. Wang, L. Duan, Y. Cui and J. Li, *Angew. Chem., Int. Ed.*, 2007, **46**, 2431–2434.
18 X. Yan, Y. Cui, Q. He, K. Wang, J. Li, W. Mu, B. Wang and Z. C. Ou-Yang, *Chemistry*, 2008, **14**, 5974–5980.
19 H. Ma, J. Fei, Q. Li and J. Li, *Small*, 2015, **11**, 1787–1791.
20 C. Huang, X. Chen, Y. Lu, H. Yang and W. Yang, *Biosens. Bioelectron.*, 2015, **63**, 478–482.
21 H. Zhang, J. Fei, X. Yan, A. Wang and J. Li, *Adv. Funct. Mater.*, 2015, **25**, 1193–1204.
22 H. H. Kohler, Thermodynamics of Adsorption from Solution, in *Coagulation and Flocculation*, CRC Press, 2nd edn, 2005, pp. 1–41.
23 M. Castelnovo and J.-F. Joanny, *Langmuir*, 2000, **16**, 7524–7532.
24 N. Dim, M. Perepelyuk, O. Gomes, C. Thangavel, Y. Liu, R. Den, A. Lakshmikuttyamma and S. A. Shoyele, *J. Nanobiotechnol.*, 2015, **13**, 61.
25 Amides and related functional groups, www.auburn.edu/~deruija/pda1_amides.pdf, accessed January 2017.
26 I. Migneault, C. Dartiguenave, M. J. Bertrand and K. C. Waldron, *BioTechniques*, 2004, **37**, 790–802.
27 J. Kong and S. Yu, *Acta Biochim. Biophys. Sin.*, 2007, **39**, 549–559.
28 A. Barth, *Biochim. Biophys. Acta, Bioenerg.*, 2007, **1767**, 1073–1101.

29 P. I. Haris and F. Severcan, *J. Mol. Catal. B: Enzym.*, 1999, **7**, 207–221.
30 O. Bozkurt, S. Haman Bayari, M. Severcan, C. Krafft, J. Popp and F. Severcan, *Biomed. Optic Express*, 2012, **17**, 0760231–0760238.
31 K. Elfrink, J. Ollesch, J. Stöhr, D. Willbold, D. Riesner and K. Gerwert, *Proc. Natl. Acad. Sci. U. S. A.*, 2008, **105**, 10815–10819.
32 E. Goormaghtigh, J. M. Ruysschaert and V. Raussens, *Biophys. J.*, 2006, **90**, 2946–2957.
33 A. Adochitei and G. Drochioiu, *Rev. Roum. Chim.*, 2011, **56**, 783–791.
34 P. Zhu, X. Yan, Y. Su, Y. Yang and J. Li, *Chemistry*, 2010, **16**, 3176–3183.
35 B. Dinesh, M. A. Squillaci, C. Menard-Moyon, P. Samori and A. Bianco, *Nanoscale*, 2015, **7**, 15873–15879.
36 G. Kaur, L. A. Abramovich, E. Gazit and S. Verma, *RSC Adv.*, 2014, **4**, 64457–64465.
37 G. P. Dado and S. H. Gellman, *J. Am. Chem. Soc.*, 1994, **116**, 1054–1062.
38 B. Nie, J. Stutzman and A. Xie, *Biophys. J.*, 2005, **88**, 2833–2847.
39 A. Barth and C. Zscherp, *Q. Rev. Biophys.*, 2002, **35**, 369–430.
40 L. J. Bellamy, in *The Infrared Spectra of Complex Molecules: Volume Two Advances in Infrared Group Frequencies*, Springer, Netherlands, Dordrecht, 1980, Associated XH Frequencies, the Hydrogen Bond, pp. 240–292.
41 B. Dinesh, V. Vinaya, S. Raghothama and P. Balaram, *Eur. J. Org. Chem.*, 2013, **2013**, 3590–3596.
42 K. Tonan and S.-i. Ikawa, *J. Am. Chem. Soc.*, 1996, **118**, 6960–6965.
43 Y. Ogawa, Y. Arikawa, T. Kida and M. Akashi, *Langmuir*, 2008, **24**, 8606–8609.
44 W. K. Lim, J. Rosgen and S. W. Englander, *Proc. Natl. Acad. Sci. U. S. A.*, 2009, **106**, 2595–2600.
45 S. Woelki and H. H. Kohler, Surface Charge and Surface Potentia, in *Coagulation and Flocculation*, CRC Press, 2nd edn, 2005, pp. 43–70.
46 K. Qiao, H. Liu and N. Hu, *Electrochim. Acta*, 2008, **53**, 4654–4662.
47 N. V. Churaev, V. D. Sobolev, T. B. Ermakova and I. P. Sergeeva, *Colloid J.*, 2004, **66**, 378–380.
48 Y.-K. Oh and T. G. Park, *Adv. Drug Delivery Rev.*, 2009, **61**, 850–862.
49 M. S. Bakshi, S. Sachar, T. Yoshimura and K. Esumi, *J. Colloid Interface Sci.*, 2004, **278**, 224–233.
50 G. von Helden, T. Wyttenbach and M. T. Bowers, *Science*, 1995, **267**, 1483–1485.
51 Y. Deng, J. B. Dixon and G. N. White, *Colloid Polym. Sci.*, 2006, **284**, 347–356.
52 M. Zaucha, Z. Adamczyk and J. Barbasz, *J. Colloid Interface Sci.*, 2011, **360**, 195–203.
53 J. Hierrezuelo, A. Sadeghpour, I. Szilagyi, A. Vaccaro and M. Borkovec, *Langmuir*, 2010, **26**, 15109–15111.
54 A. Elbakry, A. Zaky, R. Liebl, R. Rachel, A. Goepferich and M. Breunig, *Nano Lett.*, 2009, **9**, 2059–2064.
55 A. Mirtič and J. Grdadolnik, *Biophys. Chem.*, 2013, **175**, 47–53.
56 M. Dominska and D. M. Dykxhoorn, *J. Cell Sci.*, 2010, **123**, 1183–1189.
57 S. Akhtar and I. F. Benter, *J. Clin. Invest.*, 2007, **117**, 3623–3632.
58 J. Zabner, A. J. Fasbender, T. Moninger, K. A. Poellinger and M. J. Welsh, *J. Biol. Chem.*, 1995, **270**, 18997–19007.
59 I. Koltover, T. Salditt, J. O. Radler and C. R. Safinya, *Science*, 1998, **281**, 78–81.
60 S. P. Persengiev, X. Zhu and M. R. Green, *RNA*, 2004, **10**, 12–18.